A Finite Element Model for Three-Dimensional Eddy Current NDT Phenomena

NATHAN IDA, MEMBER, IEEE, AND WILLIAM LORD, SENIOR MEMBER, IEEE

Abstract—**The defect detection mechanism for eddy current nondestructive testing (NDT) probes is related to the interaction of induced eddy currents in the metal test specimen with flaws and the coupling of these interaction effects with the moving test probe. To date, numerical modeling of these phenomena has been limited to two-dimensional and axisymmetric geometries. A three-dimensional magnetic vector potential finite element formulation for the modeling of eddy current NDT phenomena is described, and the technique is illustrated by predicting differential eddy current probe impedance plane trajectories for flaws in PWR steam generator tubing.**

INTRODUCTION

NUMERICAL ANALYSIS techniques such as the finite element method have been successfully developed for the study of dc and low-frequency electromagnetic fields in electrical machines [1]–[4] and large magnet structures for fusion applications [5]. The finite element method has been shown to have certain advantages, including ease of handling boundary conditions and the ability to follow awkwardly shaped boundaries [6]. These factors are of particular importance for the simulation of electromagnetic nondestructive testing (NDT) techniques, and hence parallel developments have taken place in the use of finite element analysis for modeling electromagnetic NDT phenomena [7]–[9].

Following the success of a variety of two-dimensional and axisymmetric formulations both for machine applications and NDT models, research has concentrated on the development of more general three-dimensional formulations. The general magnetostatic problem has been handled by the use of scalar potentials [10]–[13], the magnetic vector potential [14]–[16], and integral formulations [17]. More recently, a three-dimensional numerical model for magnetostatic NDT phenomena based on the magnetic vector potential formulation has been reported [18], [20]. While magnetostatic problems can now be solved satisfactorily, the solution of eddy current problems is still under active research and subject to some controversy.

The choice of functions suitable for formulation is larger [21], [22] and many of these have been tried with varying degrees of success [23]–[26]. In many applications the use of a scalar potential in regions free of current sources is preferred because of the more economical solution obtained (in terms of computer resources). In current source regions a vector potential is necessary [21], [22], and the boundaries between the two potentials have to be coupled. The magnetic vector potential used in this formulation is less economical in terms of computer resources but is more general and avoids the need of interface coupling. It is therefore a natural choice for NDT problems where the conductor interfaces may be of a very complicated shape.

In spite of the complicated shapes of conducting regions such as defects, the fields are usually very tight around the current sources (eddy current coils). This is important since in most cases the outer boundaries can be assumed to have zero boundary conditions in terms of the magnetic vector potential. Although the controversy associated with the uniqueness of the general solution using the magnetic vector potential still persists [27]–[29] there seems to be a general agreement that under the foregoing conditions the solution is indeed unique [28]–[30].

This paper presents a new numerical procedure for eddy current problems associated with general eddy current calculations. It uses isoparametric hexahedral elements and a frontal solution routine for the elimination and back-substitution processes. The method presented is tested and compared to two-dimensional finite element calculations for accuracy and convergence and to experimental data obtained from three-dimensional defects in conducting media. In addition, the paper demonstrates the successful application of the numerical technique to moving coil problems.

Special attention has been given to the computing aspects of the model, including the use of a vector computer. This demonstrates the feasibility of such a model in a practical situation.

ELECTROMAGNETIC FIELD EQUATIONS

The differential equations governing general time-varying electromagnetic fields at low frequencies in regions that include magnetic and conducting materials and impressed current densities are derived from Maxwell's equations:

$$\nabla \times \bar{E} = -\frac{\partial \bar{B}}{\partial t} \tag{1}$$

$$\nabla \times \bar{H} = \bar{J} \tag{2}$$

Manuscript received June 5, 1984; revised May 5, 1985. This work was supported by the Electric Power Research Institute as Project RP 1395-2.

N. Ida was with the Department of Electrical Engineering, Colorado State University, Fort Collins, CO 80523. He is now with the Department of Electrical Engineering, University of Akron, Akron, OH 44325.

W. Lord is with the Department of Electrical Engineering, Colorado State University, Fort Collins, CO 80523.

0018-9464/85/1100-2635$01.00 © 1985 IEEE

$$\nabla \cdot \bar{B} = 0 \tag{3}$$

$$\nabla \cdot \bar{D} = 0. \tag{4}$$

In these equations both the displacement currents and charge density are neglected. In addition, the following constitutive relations describe the material media

$$\bar{B} = \mu \bar{H} \tag{5}$$

$$\bar{D} = \epsilon \bar{E} \tag{6}$$

$$\bar{J} = \sigma \bar{E}. \tag{7}$$

In these relations, μ, σ, and ϵ are generally tensors, but in this formulation they are assumed to be single valued in each element. Spatial variations in conductivity and permeability within each element are possible, but field dependency is not allowed.

Substituting (4) and (7) in (2) yields

$$\nu \nabla \times \bar{B} = \sigma \bar{E} \tag{8}$$

where $\nu = 1/\mu$.

The magnetic flux density can be expressed in terms of the magnetic vector potential $\bar{A}$

$$\bar{B} = \nabla \times \bar{A}. \tag{9}$$

From (1) it follows that the electric field differs from the magnetic vector potential by an irrotational vector $\nabla\phi$, ϕ being the electric scalar potential

$$\bar{E} = -\frac{\partial \bar{A}}{\partial t} - \nabla\phi. \tag{10}$$

Substituting (9) and (10) in (8) yields

$$\nu \nabla \times (\nabla \times \bar{A}) = -\sigma \frac{\partial \bar{A}}{\partial t} - \sigma \nabla\phi \tag{11}$$

or, using the vector identity $\nabla \times (\nabla \times \bar{A}) = \nabla(\nabla \cdot \bar{A}) - \nabla^2 \bar{A}$,

$$\nu(\nabla^2 \bar{A} - \nabla(\nabla \cdot \bar{A})) = \sigma \frac{\partial \bar{A}}{\partial t} + \sigma \nabla\phi. \tag{12}$$

From (7), (10), and (12), for any nonzero conductivity it follows that ϕ must satisfy [18]

$$\nabla^2 \phi = -\frac{\partial}{\partial t}(\nabla \cdot \bar{A}). \tag{13}$$

Equations (11) and (13) are a coupled system that can be solved for the three components of the magnetic vector potential $\bar{A}$ and the scalar potential ϕ everywhere in the solution region.

Under the assumptions made in this formulation, the scalar potential can arise only due to the impressed current densities. In this case, (11) and (13) become uncoupled, and the following equation is sufficient [18]:

$$\nu \nabla \times (\nabla \times \bar{A}) = -\sigma \frac{\partial \bar{A}}{\partial t} + \bar{J}_s \tag{14}$$

where $\bar{J}_s$ denotes the source current density.

Under sinusoidal steady-state conditions the magnetic vector potential is a phasor, and its time derivative can be written as

$$\frac{\partial \bar{A}}{\partial t} = -j\omega \bar{A}, \tag{15}$$

and (14) becomes

$$\nu \nabla \times (\nabla \times \bar{A}) = -j\omega\sigma \bar{A} + \bar{J}_s. \tag{16}$$

In this equation, the divergence of $\bar{A}$ has not been specified explicitly, but the gradient of ϕ is implicit in $\bar{J}_s$.

Three-Dimensional Finite Element Formulation

The finite element formulation of (16) can be based on Galerkin's method [23] or on an appropriate variational functional equivalent to (16). This latter method is adopted here.

A functional can be written in terms of the components of the magnetic vector potential $\bar{A}$, the flux density $\bar{B}$, and the current denisty $\bar{J}$ [19]:

$$F(A) = \int_V \{\tfrac{1}{2}[\nu_x B_x^2 + \nu_y B_y^2 + \nu_z B_z^2] - [J_x A_x + J_y A_y + J_z A_z] + \tfrac{1}{2} j\omega\sigma[A_x^2 + A_y^2 + A_z^2]\}\, dv \tag{17}$$

where $\bar{B}$, $\bar{A}$, and $\bar{J}$ are complex vectors. The derivation of Euler's equations and the natural boundary conditions for this functional have been described elsewhere [19] and are not repeated here.

The functional in (17) is derived based on the phasor transformation which converts a parabolic type equation (i.e., (14)) into an elliptic equation (i.e., (16)). Unlike the functional derived for magnetostatic applications [14], [20], this functional is nonextremal, and the solution is based on finding a stationary point about $\bar{A}$.

The volume of interest is now discretized into a number of eight-node hexahedral isoparametric elements. The magnetic vector potential is approximated at each node in the volume by a set of shape functions N_i:

$$A = \sum_{i=1}^{K} N_i A_i \tag{18}$$

where K is the number of nodal points in each finite element.

This approximation is now substituted into the functional (17). Taking the first derivative with respect to each unknown,

$$\frac{\partial F(A)}{\partial A_{ik}} = 0, \tag{19}$$

one reaches the standard finite element equation for an element:

$$[[K]_e + j\omega\sigma[R]_e]\,\{A\}_e = \{Q\}_e \tag{20}$$

where $[K]$ is a 24 × 24 matrix representing the real part of the stiffness matrix. $[R]$ is a 24 × 24 matrix of the

imaginary part, $\{A\}$ is the 24 × 1 vector of unknowns, and $\{Q\}$ is the 24 × 1 vector of applied currents calculated at the nodal points of the element.

The elemental contributions of the form in (20) are now calculated using an eight-point Gaussian quadrature and summed into a global system of equations of the form

$$[G]\{A\} = \{Q\} \tag{21}$$

where

$$[G] = [[K] + j\omega\sigma[R]].$$

The next step is the application of boundary conditions to the global system and solution using Gaussian elimination.

The system in (21) is both symmetric and banded the size of $[G]$ being $3N * (3 * BW)$ where BW is the semi-bandwidth of the system. Similarly, $\{A\}$ and $\{Q\}$ are of size $3N*1$ where N is the total number of nodal points in the solution region. The matrix $[G]$ is too large to be stored in a computer's memory for any realistic problem both because of the large number of nodal points and the large bandwidth of such systems. Therefore, a frontal method of assembly and elimination has been adopted.

Calculations with the Magnetic Vector Potential

From the values of the magnetic vector potential various quantities such as flux densities, eddy current densities, stored and dissipated energies and coil impedances can be calculated. The eddy current density is calculated directly from the magnetic vector potential using the equation:

$$\bar{J}_e = -j\omega\sigma\bar{A}. \tag{22}$$

Thus the three components of $\bar{J}_e$ can be calculated everywhere in the solution region. Note, however, that $\bar{A}$ is only known at the eight nodes of each element, while the current density only has meaning within the volume of the element. The current density in any element is, therefore, found by averaging the contribution of the nodes and assuming it to be constant within the element:

$$\bar{J}_e = -\tfrac{1}{8}\sum_{i=1}^{8} j\omega\sigma\bar{A}_i. \tag{23}$$

The dissipated energy can be calculated from the eddy current distribution in (23)

$$P_i = v_i|\bar{J}_e|^2/\sigma_i \tag{24}$$

where i denotes a single element, v_i the volume of the element i, $\bar{J}_e$ is the average eddy current density in element i, and σ_i is the conductivity of the element.

Substituting (23) and summing over the number of elements M, the total dissipated energy is

$$P = \sum_{i=1}^{M} v_i\sigma\omega^2|A_{ci}|^2 \tag{25}$$

where A_{ci} indicates the average (centroidal) value of the magnetic vector potential in element i.

The components of the flux density $\bar{B}$ are calculated using (9):

$$B_x = \frac{\partial A_z}{\partial y} - \frac{\partial A_y}{\partial z}$$
$$B_y = \frac{\partial A_x}{\partial z} - \frac{\partial A_z}{\partial x} \tag{26}$$
$$B_z = \frac{\partial A_y}{\partial x} - \frac{\partial A_x}{\partial y}.$$

The spatial derivatives $\partial/\partial x$, $\partial/\partial y$, and $\partial/\partial z$ are in fact calculated as part of the finite element solution [18] and therefore (26) is calculated with very little effort in the finite element solution program. The stored energy in the solution region can now be calculated as

$$W = \tfrac{1}{2}\sum_{i=1}^{N} (\nu_x B_{xi}^2 + \nu_y B_{yi}^2 + \nu_z B_{zi}^2) \cdot v_i. \tag{27}$$

The impedance of any source within the solution region is calculated from energy considerations. The resistance of the source (coils or any arrangement of conductors) is

$$R = \frac{P}{I^2} \tag{28}$$

where I is the rms value of the source current. Similarly, the inductance is calculated from the stored energy

$$L = \frac{W}{I^2}. \tag{29}$$

The source impedance is therefore

$$Z = R + j\omega L = \frac{1}{I^2}(P + j\omega 2W). \tag{30}$$

Results

To test the validity of this formulation, it has been applied to both two- and three-dimensional problems. In the two-dimensional solutions, the results from the three- and two-dimensional calculations are compared directly. This method allows an evaluation of the accuracy as well as the convergence of the solution as the number of elements increases. In the three-dimensional case, the results are compared with experimental data.

The first problem tested is shown in Fig. 1. A current-carrying conductor is located between two thick conducting slabs. This problem is solved in both two and three dimensions, and the eddy current density is calculated everywhere in the region using (23) and compared. Fig. 2 shows the discretization of the volume into finite elements. Because of the four-way symmetry in Fig. 1, only a quarter of the volume is discretized into 250 elements and 396 nodes to form a coarse mesh.

To form a finer mesh, 1000 elements and 1331 modes were used. The boundary conditions for this problem are summarized in Fig. 3. On the planes $Y = 0$ and $X = X_0$, zero magnetic vector potential values are imposed, these boundaries being far removed from the current source and thus having negligible field intensities. The boundaries at

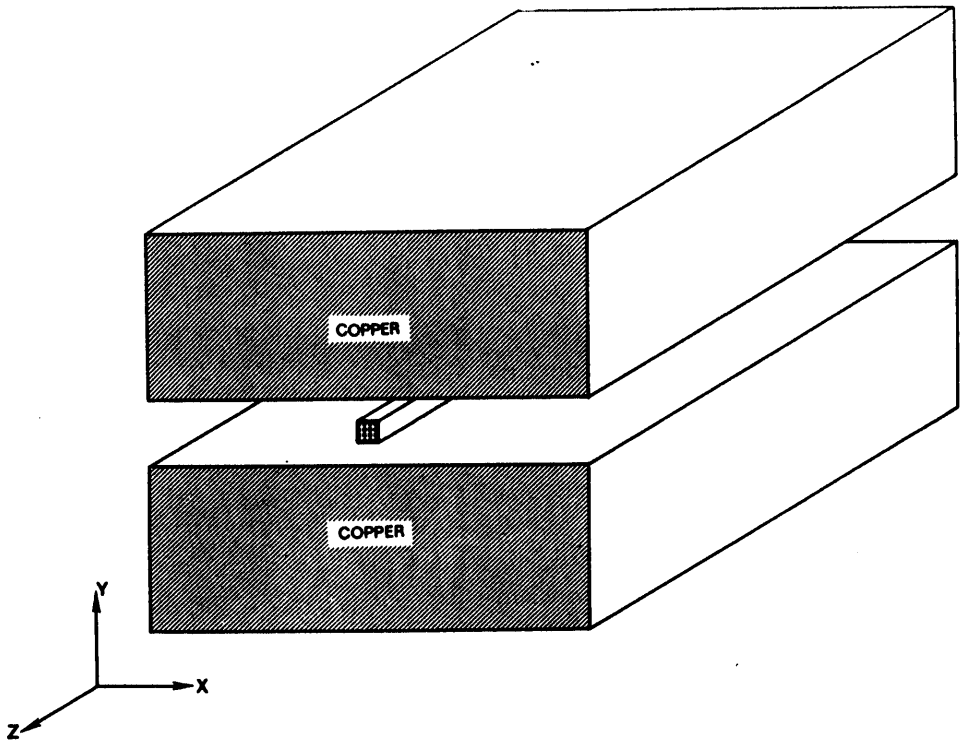

Fig. 1. Current-carrying conductor between two conducting slabs.

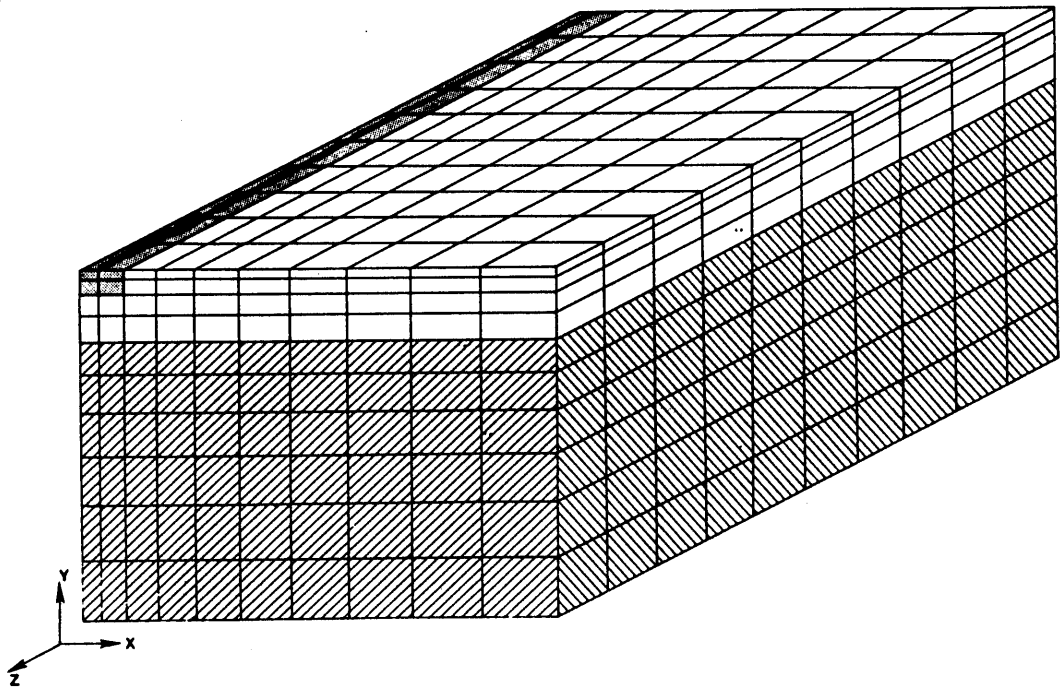

Fig. 2. Finite element discretization of geometry in Fig. 1. Because of symmetry only quarter geometry is modeled (1000 elements, 1331 nodes).

$Z = Z_0$ and $Z = 0$ could be specified by first calculating the values of $\bar{A}$ from a two-dimensional situation. This was avoided in this case because a comparison to the two-dimensional solution would tend to be more favorable than leaving the boundaries unspecified. In order to compare these results with two-dimensional calculations, two similar meshes were developed, consisting of 50 triangular elements and 36 nodes for the coarse mesh and 200 elements and 121 nodes for the finer mesh. Thus the three- and two-dimensional meshes are identical in the sense that the number of nodal points in any cross section of the three-dimensional mesh is identical with the corresponding two-dimensional mesh. Furthermore, the nodal points are located at identical coordinates.

For each of the different situations (two- and three-dimensional solutions for two different meshes) the mag-

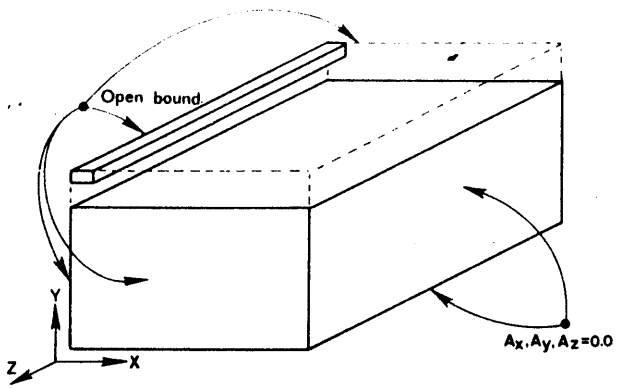

Fig. 3. Boundary conditions for conductor between slabs problem.

netic vector potential was calculated together with the eddy current density directly under the conductor (on the vertical symmetry line, see Fig. 4). Fig. 4(a) shows the solution for the coarse mesh, with 36 nodes in a cross section. The third line (C) represents the exact solution expected for this problem since a fine mesh (3200 triangular elements, 1681 nodes) was used. Fig. 4(b) shows the calculation for the finer mesh with 121 nodes in the cross section. Clearly, the solution is much closer in both the two- and three-dimensional situations, as expected. It is, however, interesting to note that the two- and three-dimensional solutions converge to the exact solution from different directions. This is probably due to the use of different types of elements (triangular elements derived in local coordinates as compared to isoparametric finite elements derived in local coordinates). Fig. 5 is an attempt to quantify the error involved in these calculations. It clearly shows that the three-dimensional code errors are comparable to those of the two-dimensional calculations and that these are reduced by increasing the number of nodal points. Because of computer limitations, however, it was not possible to increase the number of nodal points to much more than 121 nodes in a cross section, and therefore the dashed line represents an expected curve and not calculated values. It is also worth mentioning that the values plotted in Fig. 5 are the largest errors calculated in Fig. 4(a) and (b).

The second problem presented here relates to the nondestructive testing of nuclear power plant steam generators. It consists of an Inconel 600 tube and a carbon steel support plate. The tube passes through the support plate with a 0.015-in clearance between the support plate and tube. Two conical pits with a base diameter of 0.1575 in (4 mm) and depth of 0.030 in (0.762 mm) are located opposite each other on the outer surface of the tube as in Fig. 6. This particular arrangement provides symmetry while remaining three-dimensional. In reality, drilling a perfect conical pit is almost impossible. Two conical pits with a small base diameter of 0.010 in (0.25 mm) are therefore modeled, and the corresponding calculated output is compared to experimental output from identical machined pits. Two separate situations are modeled:

1) the tube with the conical pits but without the carbon steel support plate, and

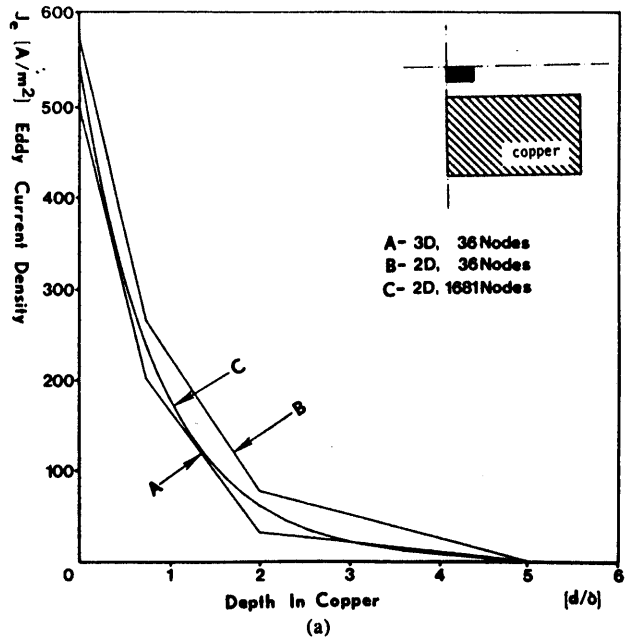

(a)

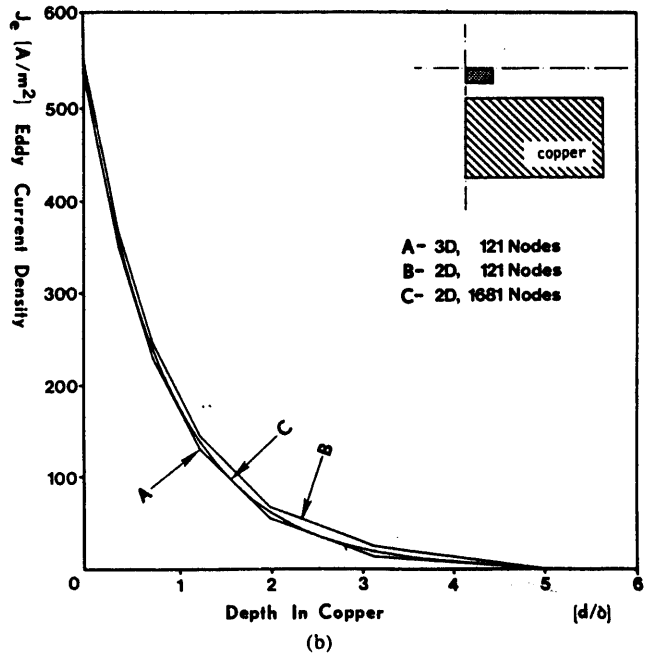

(b)

Fig. 4. Comparison of two- and three-dimensional solutions. (a) Coarse mesh (250 elements, 396 nodes). (b) Finer mesh (1000 elements, 1331 nodes).

2) the tube, conical pits, and the support plate as in Fig. 6.

This problem is unique not only in being three-dimensional but also in the fact that to produce an impedance plane trajectory, it is necessary to move the eddy current probe past the defects (pits). Thus a series of calculations are required. This is done by calculating the probe impedance at a particular position, then moving the probe to a new position and calculating the corresponding impedance. This is continued for a relatively large number of positions thus obtaining an "impedance plane trajectory." This trajectory is representative of the particular flaw present and therefore is a very important tool in the evaluation of NDT results.

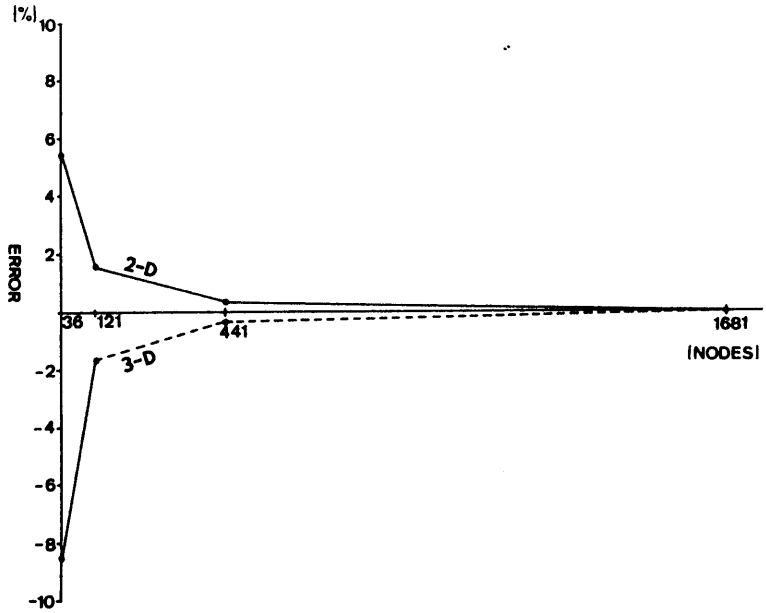

Fig. 5. Comparison of errors in two- and three-dimensional solutions, for conductor between slabs problem at different discretization levels. Number of nodes in three-dimensional case indicates the number of nodes in a cross section.

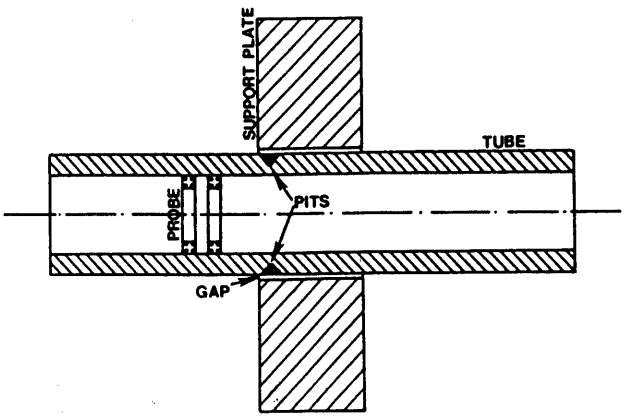

Fig. 6. Steam generator geometry showing an Inconel 600 tube, support plate, and eddy current probe. Two conical pits are shown under edge of support plate.

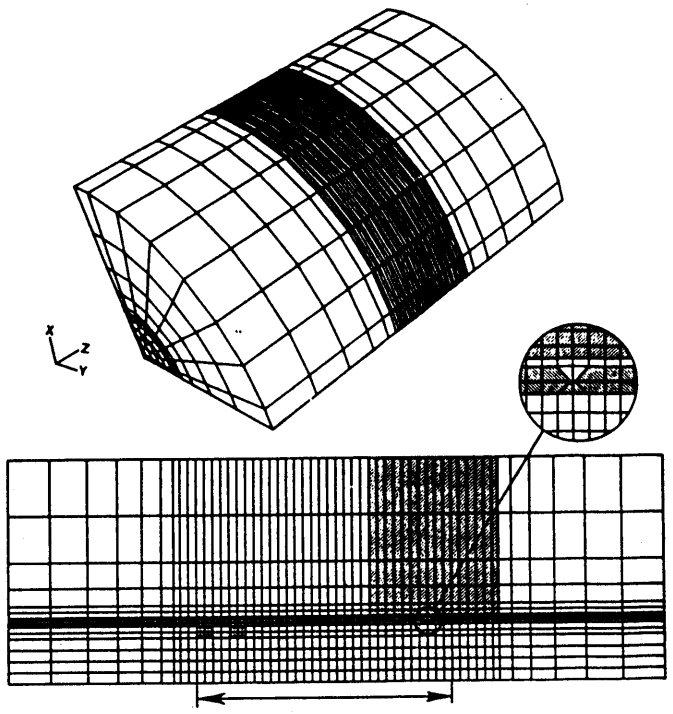

Fig. 7. Finite element discretization of steam generator geometry. Total of 5408 elements and 6572 nodes were used to model quarter of geometry. (a) total mesh with hidden lines removed. (b) Cross section through mesh at $Y = 0$, showing tube, support plate, and pits. Probe moves in section indicated by arrows with total of 24 probe positions.

Fig. 7 shows the mesh for this problem. It consists of a total of 5408 eight-node elements and 6572 nodes. Because of the symmetry mentioned earlier, only a quarter of the geometry is modeled. Fig. 7(a) shows a view of the mesh with hidden lines removed showing the location of the tube and support plate. Fig. 7(b) is a view of the plane $X = 0$ and shows the coils of the differential probe, the tube and support plate, and the location of the conical pit. The region of probe movement is indicated by the two arrows in Fig. 7(b).

The boundary conditions for this problem are as follows. On the outer curved boundary and on the planes $Z = 0$ and $Z = Z_0$, zero boundary conditions are applied for all three components of the magnetic vector potential. The assumption is that these boundaries are far removed from the source (eddy current coils). The boundaries at $X = 0$ and $Y = 0$ are symmetry planes and therefore can be left unspecified. The current in the coils at these boundaries crosses at 90°, and therefore, at the boundaries in the absence of any discontinuity, the tangential components of $\bar{A}$ are zero while the normal component can be left unknown or calculated from an axisymmetric formulation. In this application, only the normal components on the plane $Y = 0$ were specified as zero and the rest left unspecified.

The problem is solved for 24 probe positions. In the first case, where only the conical pits are modeled, the situation is also symmetric in the z direction, and the probe is

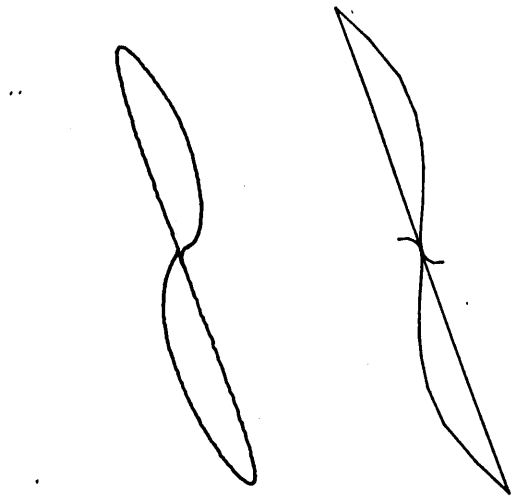

Fig. 8. Comparison of results; modeling of tube and conical pits. (a) Experimental impedance plane trajectory. (b) Finite element prediction of impedance plane trajectory.

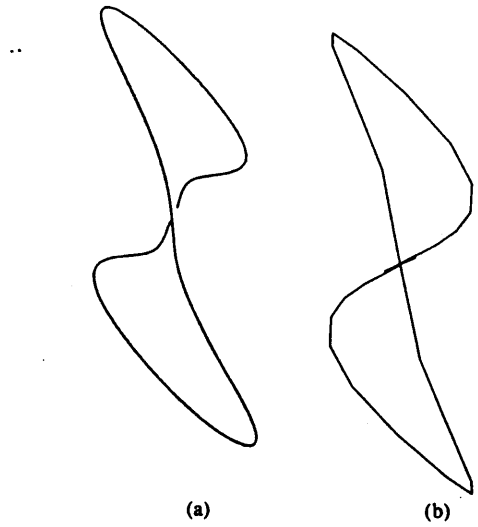

Fig. 9. Comparison of results; modeling of tube, support plate, and pits. (a) Experimental impedance plane trajectory. (b) Finite element prediction of impedance plane trajectory.

moved up to the point where it is centralized with the pit. To obtain a complete impedance plane trajectory the impedances calculated are reflected about zero and the total trajectory plotted as shown in Fig. 8. Fig. 8(a) shows the experimental trajectory and Fig. 8(b) shows the calculated trajectory. These impedance plane trajectories are normalized, and therefore only the shape is compared.

In the second case, the pit is located at the edge of the support plate as shown by the shaded area in Fig. 7(a). This was done since in practice it is known that a composite signal of the support plate and the pit results. The probe is again moved through 24 positions, up to the point where it is centralized with the support plate. In this case, the symmetry in the z direction does not exist, and therefore the impedance plant trajectory is completed by modeling the support plate itself, without the pit, and reflecting these impedances about zero. The experimental and finite element output for this situation are plotted in Fig. 9(a) and (b), respectively. It is interesting to note that the two lobes of the impedance plane trajectories in Fig. 9 are almost identical. Essentially, this means that the effect of the pit on the signal is very small both in the experimental and finite element output. This is due to the fact that these trajectories were obtained at 1 kHz. At higher frequencies the effect of the pit is enhanced, but modeling at higher frequencies requires a larger number of elements due to the reduced skin depth.

It is also worth noting that the largest error occurs around the origin (i.e., in the first few probe positions). This is mainly due to the fact that the boundaries of the solution region were not taken far enough from the probe. It is, however, of little importance, the error being relatively small. Another characteristic of this type of modeling is that most of the change in the impedance occurs in only a few probe positions, close to the edges of discontinuities. Thus, in Figs. 8 and 9 less than half of the probe positions form the trajectory, the rest being points close to the zero point.

Computational Considerations

In many situations where the finite element method is used, little or no consideration is given to the computer used. It is assumed that the computer is capable of storing the matrices in (29) on core and solving them quickly with little computational error. This is certainly the case in many two-dimensional problems. Even if the number of nodal points is large, the bandwidth of the global matrix is usually small, and the solution time is reasonable.

In contrast, in three-dimensional problems of the type described here the number of variables to be solved for (number of equations) is very large and so is the bandwidth. Thus, for example, the problem described earlier requires the solution of 19 716 equations with a semibandwidth of 432. To store the complex matrix $[G]$ alone, 17 Mwords of memory are required. Such vast memories are beyond the capacity of any computer, and therefore it is necessary to use off-core storage in one way or another.

The approach used in this work consists of the use of an efficient frontal technique that uses skyline storage. This, together with a large magnetic disk (or even a magnetic tape) overcomes the shortage of real memory but it is done at the expense of solution time.

The results in Figs. 8 and 9 were obtained using a Cyber 205 vector computer. By using the vector instruction available and efficient I/O, the solution time can be reduced to acceptable levels. Table I summarizes the solution times obtained for the current results and also compares the performance of the Cyber 205 and a VAX 11/780 for a similar problem with a smaller number of elements and nodal points. This problem had 3360 elements and 4171 nodes. This resulted in a system of 12 513 equations with a bandwidth of 342. A few points are worth comment in this table.

First, the solution time and resources needed for mesh generation are insignificant in all cases as compared to the solution time. Similarly, most of the CPU time is spent in the elimination process, while most of the I/O time is used

TABLE I
COMPARISON OF PERFORMANCE OF A VAX 11/780 AND A CYBER 205 VECTOR COMPUTER[a]

	12 513 Variables VX 11/780	12 513 Variables Cyber 205	19 716 Variables Cyber 205
Mesh generator	4 min, 57 s	16 s	28 s
Elimination	12 h, 20 min		
Backsubstitution one step	22 min		
Backsubstitution[b]	8 h, 48 min		
Total	21 h, 13 min	29 min, 54 s	66 min, 16 s
Total clock time	approx. 82 h	30 min, 10 s	66 min, 44 s

[a] The third column refers to the generator geometry modeled in this work.
[b] Twenty-four steps.

in the backsubstitution process. In the case of the Cyber 205, no information is available on the various steps, but the total time is significantly reduced (to about 0.6 percent of the time required on the VAX 11/780 for the same problem). Note that the VAX 11/780 was used in a single-user mode for this particular problem. Second, the size of problems solvable on the Cyber 205 is significantly larger, and they can be solved in reasonably short times.

Also note that the results presented here only represent the first step in moving from a conventional computer to a vector environment. Thus, for example, the program on the VAX 11/780 was used on the Cyber 205 with minor changes and only minimum vectorization. In addition, since the results on both computers were identical (although the Cyber 205 uses a 64-bit word as compared to the 32-bit word used by the VAX 11/780) one could use half-words (32-bit) on the Cyber 205, effectively speeding the operations by a factor of two and reducing storage by a factor of two. In the next step, the algorithm itself should be modified to take advantage of more of the vector instructions available on vector computers.

Another significant aspect in three-dimensional analysis is computer graphics. Although it is important in any dimension, two-dimensional analysis requires only modest line plotting capabilities. In three dimensions, hidden line removal (Fig. 7(a)), rotation, cut sections through the mesh (Fig. 7(b)), and others are indispensible if the vast data set generated in the solution process is to be manageable.

CONCLUSION

The numerical model outlined in this paper is capable of predicting the necessary parameters for a complete nondestructive evaluation process. In the examples given here, only the coil impedances for a differential probe are calculated. Other situations such as absolute eddy current probes, permeability, and conductivity values around defects can be evaluated. Indeed, any parameter in the field equations can be calculated for given values of the other parameters. The examples given in this work are taken from the nondestructive testing field, but the model is applicable to a wide range of situations that fall within the assumptions made in this formulation.

The solution times obtained, especially with the Cyber 205 vector computer, are well within acceptable limits and can be further reduced by proper algorithm development. This, coupled with the new developments in the finite element method such as infinite elements, should bring the solution of large moving probe problems within the practical realm.

REFERENCES

[1] A. M. Winslow, "Numerical solution of the quasilinear poisson equation in an nonuniform triangle mesh," *J. Computational Phys.*, vol. 2, pp. 149-172, 1967.
[2] P. Silvester and M. V. K. Chari, "Finite element solution of saturable magnetic field problems," *IEEE Trans. Power App. Syst.*, vol. PAS-89, pp. 1642-1651, 1970.
[3] J. Donea, S. Giuliani, and A. Philippe, "Finite elements in the solution of electromagnetic induction problems," *Int. J. Numer. Methods Eng.*, vol. 8, pp. 359-367, 1974.
[4] O. W. Anderson, "Transformer leakage flux program based on the finite element method," *IEEE Trans. Power App. Syst.*, vol. PAS-92, pp. 682-689, Mar./Apr. 1973.
[5] C. W. Trowbridge, "Three-dimensional field computation," *IEEE Trans. Magn.*, vol. MAG-18, pp. 293-297, Jan. 1982.
[6] N. A. Demerdash and T. W. Nehl, "An evaluation of the methods of finite elements and finite differences in the solution of nonlinear electromagnetic fields in electrical machines," *IEEE Trans. Power App. Syst.*, vol. PAS-98, pp. 74-87, Jan./Feb. 1979.
[7] W. Lord, "A survey of electromagnetic methods of nondestructive testing," in *Mechanics of Nondestructive Testing*, W. W. Stinchcomb, Ed. New York: Plenum Press, 1980, ch. 3, pp. 77-100.
[8] W. Lord and J. H. Hwang, "Finite element modeling of magnetic field/defect interactions," *ASTM. J. Testing Evaluation*, vol. 3, pp. 21-25, Jan. 1975.
[9] W. Lord and R. Palanisamy, "Development of theoretical models for NDT eddy current phenomena," in *Eddy Current Characterization of Materials and Structures*, G. B. Birnbaum and G. Free, Eds., ASTM, ASTM STP 722, 1981, pp. 5-21.
[10] O. C. Zienkiewicz, J. Lyness, and R. J. Owen, "Three-dimensional magnetic field determination using a scalar potential—A finite element solution," *IEEE Trans. Magn.*, vol. MAG-13, pp. 1649-1655, Sept. 1977.
[11] J. Simkin and C. W. Trowbridge, "Three-dimensional nonlinear electromagnetic field computations using scalar potentials," *Proc. Inst. Elec. Eng.*, vol. 127, Part B, pp. 368-374, Nov. 1980.
[12] J. Simkin and C. W. Trowbridge, "On the use of the total scalar potential in the numerical solution of field problems in electromagnetics," *Int. J. Numer. Methods in Eng.*, pp. 423-440, 1979.
[13] K. R. Davey and E. I. King, "A three dimensional scalar potential field solution and its application to the turbine generator end region," *IEEE Trans. Power App. Syst.*, vol. PAS-100, pp. 2302-2310, May 1981.
[14] N. A. Demerdash, T. W. Nehl, F. A. Fouad, and O. A. Mohammed, "Three dimensional finite element vector potential formulation of

magnetic fields in electrical apparatus," *IEEE Trans. Power App. Syst.*, vol. PAS-100, pp. 4104-4111, Apr. 1981.

[15] S. Aoki, "Three-dimensional magnetic field calculation of the levitation magnet for HSST by the finite element method," *IEEE Trans. Magn.*, vol. MAG-16, pp. 725-727, Sept. 1980.

[16] M. V. K. Chari, Z. J. Cendes, P. P. Silvester, A. Konrad, and M. M. Palmo, "Three-dimensional magnetostatic field analysis of electrical machinery by the finite element method," *IEEE Trans. Power App. Syst.*, vol. PAS-100, pp. 4007-4019, Aug. 1981.

[17] J. Simkin and C. W. Trowbridge, "Magnetostatic fields computed using an integral equation derived from Green's theorems," in *Proc. Compumag Conf.*, 1976, pp. 5-14.

[18] N. Ida, "Three dimensional finite element modeling of electromagnetic nondestructive testing phenomena," Ph.D. dissertation, Colorado State Univ., Fort Collins, Spring 1983.

[19] N. A. Demerdash, O. A. Mohammed, T. W. Nehl, F. A. Fouad, and R. H. Miller, 'Solution of eddy current problems using three dimensional finite element complex magnetic vector potential," *IEEE Trans. Power App. Syst.*, vol. PAS-101, pp. 4222-4229, 1982.

[20] N. Ida and W. Lord, "3-D finite element predictions of magnetostatic leakage fields," *IEEE Trans. Magn.*, vol. MAG-19, pp. 2260-2265, Sept. 1983.

[21] M. L. Brown, 'Calculation of 3-dimensional eddy currents at power frequencies," *Proc. Inst. Elec. Eng.*, vol. 129, Part A, pp. 46-53, Jan. 1982.

[22] P. Hammond, "Use of potentials in calculation of electromagnetic fields," *Proc. Inst. Elec. Eng.*, vol. 129, Part A, pp. 106-112, Mar. 1982.

[23] C. S. Biddlecomb, E. A. Heighway, J. Simkin, and C. W. Trowbridge, "Methods for eddy current computation in three dimensions," *IEEE Trans. Magn.*, vol. MAG-18, pp. 492-497, Mar. 1982.

[24] T. W. Preston and A. B. J. Reece, "Solution of 3-dimensional eddy current problems: The T-method," *IEEE Trans. Magn.*, vol. MAG-18, pp. 486-491, Mar. 1982.

[25] C. J. Carpenter, "Composition of alternative formulations of 3-dimensional magnetic-field and eddy-current problems at power frequencies," *Proc. Inst. Elec. Eng.*, vol. 124, pp. 1026-1034, 1977.

[26] B. Ancelle and J. C. Sabonnadiere, "Numerical solution of 3-D magnetic field problems using boundary integral equations," *IEEE Trans. Magn.*, vol. MAG-16, pp. 1089-1091, 1980.

[27] Z. J. Cendes, J. Weiss, and S. R. H. Hoole, "Alternative vector potential formulations of 3-D magnetostatic problems," *IEEE Trans. Magn.*, vol. MAG-18, pp. 367-372, Mar. 1982.

[28] J. Weiss and C. J. Cendes, "On the uniqueness of the vector potential formulation for three dimensional magnetostatic field problems," presented at the Compumag Conf., Santa Margherita, Italy, May 1983.

[29] N. A. Demerdash, T. W. Nehl, O. A. Mohammed, and F. A. Fouad, "Experimental verification and application of the three dimensional finite element magnetic vector potential method in electrical apparatus," *IEEE Trans. Power App. Syst.*, vol. PAS-100, pp. 4112-4122, Aug. 1981.

[30] J. R. Brauer, R. Y. Bodine, and L. A. Larkin, "Nonlinear anistropic three dimensional magnetic energy functional," presented at the Compumag Conf., Santa Margherita, Italy, May 1983.